Int. J. Heat Mass Transfer. Vol. 32, No. 5, pp. 795–810, 1989
Printed in Great Britain

0017–9310/89 $3.00+0.00
Pergamon Press plc

Transient radiative–conductive heat transfer in flat glasses submitted to temperature, flux and mixed boundary conditions

TAN HE PING† and M. LALLEMAND
Laboratoire de Thermique, ENSMA, LESTE, UA 1098, Rue Guillaume, VII, 86034 Poitiers Cédex, France

(*Received* 29 *January* 1988 *and in final form* 23 *June* 1988)

Abstract—A nodal analysis based on Hottel's zonal method extended by the ray tracing method is carried out in order to treat the transient combined radiative–conductive heat transfer one-dimensional problem, in non-grey semi-transparent materials—more especially glasses—submitted to several thermal and radiative boundary conditions. Coupling problems for the prescribed temperatures, prescribed radiative–convective heat exchange laws and mixed kind thermal boundary are worked out for opaque as well as vitreous interfaces with specular reflections. The effects of variations of the influence parameters, Planck number, Biot number, Fourier number, emissivities of the slab and refractive index of the medium are considered. Two applications of the numerical modelling are studied: predictions of the temporal behaviour of a fused silica windshield mounted on a spacecraft engine during re-entry, and the simulation of the transient transfer in a glass melt in contact on one side with a metallic bath and submitted to radiative–convective exchanges on the opposite side.

1. INTRODUCTION

So FAR, a review of previous work on transient combined radiative–conductive heat transfer in semi-transparent materials (STM) with flux boundary conditions shows little interest among the heat transfer community. However, thoroughly practical and economical consequences are considered. Among the various fields of application, one can mention:

(a) in glass technology, for the mastery of annealing and quenching operations,

(b) in space engineering, for the re-entry of spacecraft in the atmosphere,

(c) in nuclear engineering, for cooling processes of nuclear fuel devices and control of the energy release in vitrified nuclear wastes,

(d) in solar energy, for devices having to hold a daily and nocturnal rhythm.

Earlier studies on transient coupled radiative–conductive heat transfer in STM were carried out mainly for the boundary conditions of the first kind—i.e. with prescribed temperatures at the frontiers—and they were summarized by Viskanta and Anderson [1]. For industrial purposes, Chui and Gardon [2] undertook the study of combined transfer in grey glass baths including asymmetric flux boundary conditions. Doornink and Hering [3] worked out the rigorous analysis of the wall problem in the frame of a grey medium bounded by black frontiers. Weston and Hauth [4] broadened the preceding work for the case of an isotropic scattering medium fitted with two non-black surfaces by using the discrete directional method. Lauriat [5] investigated the same problem in an absorbing–emitting–scattering grey medium with non-black radiative boundaries by iterative integration of the Fredholm equation. Saulnier [6], by means of nodal analysis and a thermal network analyser, determined the transient temperature field in a plane parallel grey wall when a radiant heat pulse impinges one of its black frontiers. Sutton [7] has especially considered the grey problem at short times by a hybrid Galerkin-iterative/finite difference scheme. Very recently, Glass *et al.* [8] treated the case of a grey wall bounded by coated surfaces upon which external radiative flux may be imposed.

The combined heat transfer problem within a wall of STM bounded by semi-transparent frontiers has been investigated for a non-grey layer in the permanent situation by Bityukov *et al.* [9]. Viskanta and Kim [10] and Ramerth and Viskanta [11] have proposed a model of simultaneous transfer, in the steady state, for a coal ash deposit, fits with opaque/semi-transparent boundaries. Kuriyama *et al.* [12] have studied the modelling, by a transient finite difference method, of a non-grey glass slab with natural frontiers, heated externally by radiation. Burka [13] deduced a numerical solution of the same problem by integration of non-linear integral equations for spectral and temperature-dependent optical properties.

This paper presents an investigation of the transient behaviour of a non-grey STM slab—more particularly industrial glasses—held at high temperature, subjected to various radiative conditions (opaque or transparent, specular or diffuse) and thermal boundary conditions (first, third and mixed kinds). With this aim, a model has been built which is able to determine temperature and flux profiles of the (one-

† Present address: Harbin Institute of Technology, Harbin, People's Republic of China.

NOMENCLATURE

a — thermal diffusivity, $\lambda/(\rho C_p)$ [$m^2 s^{-1}$]
a_{k,T_i} — fractional spectral emissive power of spectral band k at nodal temperature T_i
Bi_1, Bi_2 — Biot number at $\xi = 0$, $(h_1\delta/\lambda)$, and $\xi = 1$, $(h_2\delta/\lambda)$, respectively, $\delta = d/2$
C_p — constant pressure specific heat [$J\,kg^{-1}\,K^{-1}$]
d — thickness of the slab [m]
EEA — extended exchange area
$E_n(x)$ — exponential integral function (of order n), $\int_0^1 \mu^{n-2}\,e^{-x/\mu}\,d\mu$
$F_k(z)$ — see equations (14) and (19)
$Fo, Fo(\Delta t, \Delta x)$ — Fourier number at/d^2 or the local discretized Fourier number, $a\,\Delta t/(\Delta x^2)$
F_r^*, F_t^* — dimensionless radiative heat flux and total heat flux respectively, $q^r/(\sigma T_{rf}^4)$, $q^t/(\sigma T_{rf}^4)$
h_1, h_2 — heat transfer coefficient at $\xi = 0$ and 1, respectively [$W\,m^{-2}\,K^{-1}$]
NBA — total number of spectral bands
NM — total number of nodes
N_P — Planck number, $\lambda/(4d\sigma n_M^2 T_{rf}^3)$
$n_{k,M}, n_{k,rf}$ — refractive index of STM and reference, respectively, relative to the spectral band k $(\Delta\lambda_k)$
$q_{i,e}^r q_{i,w}^r$ — local radiative heat flux at a surface situated midway between nodes i and $i+1$, nodes $i-1$ and i, respectively
$(S_iS_j)_k, (S_iV_j)_k, (V_iV_j)_k$ — extended exchange area relative to spectral band k
ST — semi-transparent ranges of the STM
TR — transparent ranges of the STM
T_i — nodal temperature [K]
T_{rf1}, T_{rf2} — reference temperatures [K]
T^* — dimensionless temperature, T/T_{rf2}
t — physical time
$t_{1,k}, t_{2,k}$ — transmissivity of surfaces S_1 and S_2, respectively, relative to spectral band k
$t^*(d), t^*(\delta)$ — dimensionless time, $Fo(d) = at/(d^2)$, $Fo(\delta) = at/(\delta^2)$, $\delta = d/2$
t_s^* — steady-state dimensionless time
$\Delta t, \Delta t^*$ — time interval and dimensionless time interval, respectively
V_i — volume relative to node i
x_{ij} — distance separating node i from node j
Δx — uniform internodal distance.

Greek symbols
δ — half thickness of slab
$\varepsilon_{1,k}, \varepsilon_{2,k}$ — emissivity of surfaces S_1 and S_2, respectively, relative to spectral band k
$\varepsilon_{-\infty}, \varepsilon_{+\infty}$ — emissivity of surfaces $S_{-\infty}$ and $S_{+\infty}$, respectively
θ_c — critical angle of reflection
Θ — dimensionless normalized temperature, $(T - T_{rf1})/(T_{rf2} - T_{rf1})$
κ_k — absorption coefficient relative to spectral band k [m^{-1}]
λ — phonic thermal conductivity [$W\,m^{-1}\,K^{-1}$]
μ — direction cosine for angle-dependent property, $\cos\theta$
μ_c — $\cos\theta_c$
$\xi, \Delta\xi$ — dimensionless distance and dimensionless spatial intervals, x/d, $\Delta x/d$
ρ — density [$kg\,m^{-3}$]
$\rho_{1,k}, \rho_{2,k}$ — reflectivity of surfaces S_1 and S_2, respectively, relative to spectral band k
$\rho_{\parallel,k}, \rho_{\perp,k}$ — directional reflectivity components respectively parallel and perpendicular to the incident plane
σ — Stefan–Boltzmann constant
$\tau_k, \tau_{0,k}$ — optical depth and optical thickness, respectively, relative to spectral band k
Φ_i^r — radiative source at node i
Φ_i^{*r} — dimensionless radiative source of node i, $\Phi_i^r/(4\sigma n_M^2 T_{rf}^4)$.

Superscripts
c, r, t — conduction, radiation and total, respectively
s — specular reflection.

Subscripts
1, 2 — refer to frontiers S_1 and S_2, respectively
$-\infty, +\infty$ — refer to frontiers $S_{-\infty}$ and $S_{+\infty}$, respectively
o–o — refers to an STM slab fitted with opaque interfaces
t–o — refers to an STM slab fitted with semi-transparent and opaque interfaces
t–t — refers to an STM slab fitted with semi-transparent interfaces.

dimensional) problem in these different situations by a combination of the nodal analysis and Hottel's zonal method extended to specular and vitreous reflection by the ray tracing method. Although the model is not able to describe polarization effects, it can take into account angular dependence of the reflectivity of dielectric–metallic interfaces. The proposed model is used, tentatively, to afford temporal and spatial descriptions of heat exchanges occurring in various thermal conditions encountered in flat glass technology and aerothermal problems in space engineering.

In Section 2 the optical properties of soda-lime silica glasses in the infra-red region are briefly described. In Section 3 the discretized energy equation scheme is introduced; after which, the determination of the radiative source is exposed for the particular case of the semi-transparent radiative boundary configuration (other radiative conditions are referred to in the Appendix). Section 4 is devoted to the numerical results when a frontier of the slab, initially at a uniform temperature, is cooled at prescribed temperatures, and the effect of the variation of the influence parameters is examined. The case of the mixed thermal and radiative boundary conditions is examined in Section 5 with applications to glass-making, and that of a wall of STM cooled symmetrically by natural convection and radiative dissipation is considered in Section 6. Finally, in Section 7 the modelling method is used to predict the transient behaviour during re-entry of a vitreous silica windshield mounted on a spacecraft.

2. THE RADIATIVE PROPERTIES OF THE STM SPECIMENS

The simplest way to consider the spectral character of an STM is to represent its different optical properties by rectangular band models: such representations are well adapted for types of glass which have low resolution spectra.

In Table 1 are reported values of the absorption spectra of various glasses described by a three or five rectangular band model. They cover a very wide range of semi-transparency, from clear optical glass to strong absorbing glass. In addition, hemispherical reflectivity and emissivity properties of silica soda-lime glasses are listed in the mid-infra-red [14]. For simplicity, the refractive index of the material was always taken without spectral effect, except in the mid-infra-red opacity range.

For a rigorous radiative energy analysis, we should have to take into account the temperature dependence of the infra-red spectrum of each STM; indeed, there is some experimental evidence, depending on the glass composition, showing that for a smelt glass, by increasing the temperature, the opacity front moves towards the visible region and the transparency of the intermediate region increases in a complicated way; but in what follows such refinements may be ignored.

The surface states of the examined glasses are assumed to be either (1) coated by a medium of strong absorption (for example, a metallic substrate), here called an 'opaque frontier', or (2) in direct contact with a non-absorbing medium of low refractive index, termed a 'semi-transparent frontier' or 'natural frontier'.

3. THE DISCRETIZED ENERGY EQUATION OF THE COMBINED RADIATIVE–CONDUCTIVE PROBLEM IN HOTTEL'S ZONE METHOD GENERALIZED BY THE RAY TRACING METHOD

A plane parallel wall of an emitting–absorbing medium confined between radiative frontiers is considered. Variable physical properties of the STM may be taken into account. For a numerical approach to the simultaneous radiative–conductive heat exchange problem, when the slab of STM is in a non-equilibrium thermal state, a nodal analysis of the coupling phenomena is worked out for the grid model of Fig. 1(a).

The wall is disposed between two black frontiers labelled $S_{-\infty}$ and $S_{+\infty}$ which simulate the radiative surrounding of the STM and which stay at fixed temperature. The slab is subdivided into NM isothermal nodes; $i = 1$ and NM denote nodes of interfaces S_1 and S_2, which may be opaque or semi-transparent to infra-red radiation; grid points $3 \leqslant i \leqslant NM-2$ are internal nodes, the internodal distance of which is Δx and grid points $i = 2$ and $NM-1$ denote nodes in the vicinity of the interface; they have internodal distance $\Delta x/2$.

In a homogeneous and isotropic medium, the transient behaviour of the temperature within the slab is governed by the energy equation

$$\rho C_p \, \partial T/\partial t = -\operatorname{div} \mathbf{q}^{t}. \tag{1}$$

In an STM, $\mathbf{q}^t$ is the total heat flux density that is the sum, $\mathbf{q}^c + \mathbf{q}^r$, of the conductive and radiative flux associated with the bi-mode exchange process.

3.1. *The discretized scheme*

The discretization of the equation of the combined radiative–conductive heat transfer problem is derived by integrating equation (1) over the control volume

Table 1. Optical characteristics of the different glasses used

λ (μm)	n	Spectrum A κ_λ (m^{-1})	Spectrum B κ_λ (m^{-1})	λ (μm)	n	$\rho_1 = \rho_2$	Spectrum C κ_λ (m^{-1})
0.5–2.7	1.5	10	2.5	0.5–1.0	1.5	0.04	10
				1.0–2.7	1.5	0.04	100
2.7–4.5	1.5	1000	250	2.7–4.3	1.5	0.04	1000
4.5–50	1.5	5000	1250	4.3–10.3	1.5	0.06	10000
				10.3–50	1.8	0.15	10000

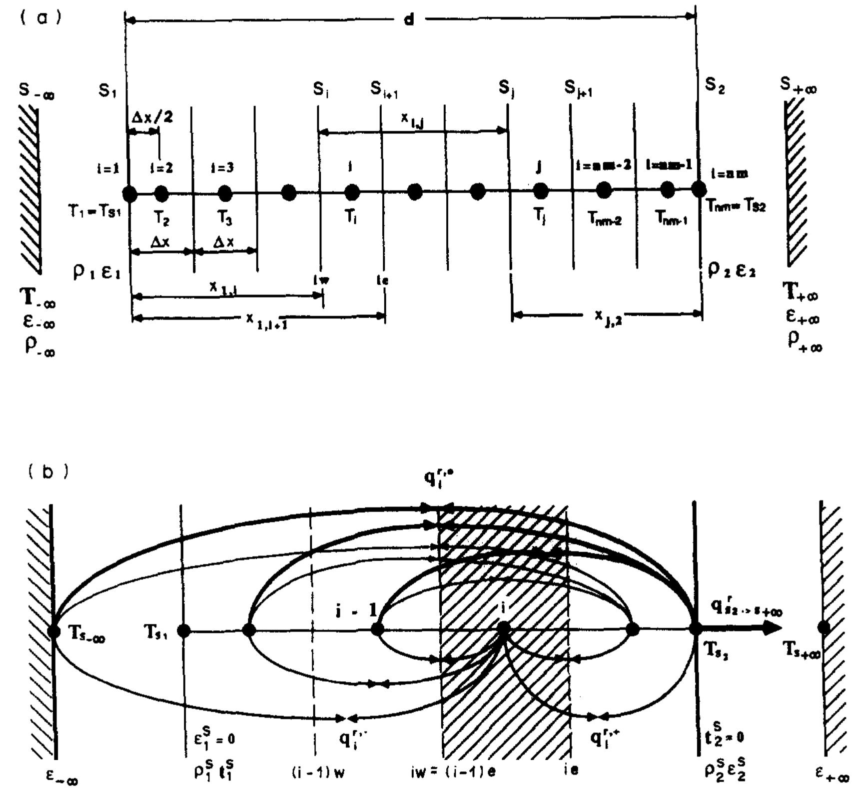

FIG. 1. (a) The infinite slab of STM modelling by the nodal method. (b) Origin of the source term, opaque frontiers/semi-transparent frontiers.

and over the time interval from t to $t+\Delta t$. Using an implicit scheme, it becomes, in reduced variables

$$T_i^{*m+1} - T_i^{*m} = Fo(T_{i+1}^{*m+1} - 2T_i^{*m+1} + T_{i-1}^{*m+1}) + Fo\,\Delta\xi\,\Phi_i^{*r,m+1}/N_P \qquad (2)$$

where Fo represents the local discretized Fourier number, N_P the Planck number defined in the non-grey sense and $\Phi^{*r} = \Phi_i^r/(4\sigma n_M^2 T_{rf}^4)$, Φ_i^r is the source term, defined as the difference between the total incoming (q_{ie}^r) and the total outgoing (q_{iw}^r) radiative flux—that is, the balance of exchanged radiative flux occurring in a prescribed control volume.

The numerical scheme of equation (2) depends on two temporal strata labelled m and $m+1$; the coupling phenomenon links, on stratum $m+1$, a node i to its adjacent nodes by conduction, and to all other distant nodes by radiation, including surfaces S_1, S_2 when frontiers are opaque, or including surfaces nodes $S_{-\infty}$, $S_{+\infty}$, when frontiers are semi-transparent in the infra-red for the transparent and semi-transparent ranges of the STM (refer to Fig. 1(b)).

3.2. *Thermal and radiative boundary conditions*

The description of the combined heat transfer should be completed by boundary conditions, taking into account temperature prescriptions or prescribed laws of heat exchanges at the interface by convective and radiative processes.

For an opaque surface, the more general form of the heat transfer boundary condition can be written at $\xi = 0$ or 1 (since $\varepsilon_{-\infty}, \varepsilon_{+\infty} = 1$)

$$\sum_{k=1}^{NBA} \varepsilon_{i,k} n_{k,rf}^2/(4n_{k,M}^2 N_P)\{a_{k,T_{si}}T_{si}^{*4} - a_{k,T_{sn}}T_{sn}^{*4}\} + 2Bi_i(\delta)(T_{si}^* - T_{sn}^*) = q_{si}^{*r}/N_P + 2(T_j^* - T_{si}^*)/\Delta\xi \qquad (3)$$

for $i = 1$ or 2, $n = -\infty$ or $+\infty$ and $j = 2$ or $NM-1$. In this equation, q_{si}^{*r} is the radiative density flux at boundary S_i. For $S_i = S_1$ one has

$$q_{s1}^* = \sigma \sum_{k=1}^{NBA} n_{k,M}^2 \left\{ \varepsilon_{1,k}(S_1 S_2)_k (a_{k,T_{s2}}T_{s2}^4 - a_{k,T_{s1}}T_{s1}^4) + \sum_{j=2}^{NM-1} \varepsilon_{1,k}(S_1 V_j)(a_{k,T_j}T_j^4 - a_{k,T_{s1}}T_{s1}^4) \right\} \Big/ (4\sigma n_M^2 T_{rf}^4). \qquad (4)$$

Equations of type (3) are consequences of the energy conservation principle. The first term on the left-hand side of equation (3) expresses the part of the energy dissipated by radiation at the interface in the opaque range of the STM and the second term is the quantity of heat gained or lost by convection processes; on the right-hand side, the first term is the local radiative flux at the frontier issuing from the slab interior and the second term expresses the conductive heat flux coming from the last two nodes. It can be noticed that boundary conditions depend on two influence parameters N_P and Bi and also on the emissivities.

Summation in equations (3) and (4) runs over the total number of spectral bands, k ($1 \leqslant k \leqslant NBA$), for, in the infra-red transparent range of the STM, surface emissivities may equal zero in these regions. For the opaque surface or the infra-red opaque region of the spectrum of a semi-transparent surface, the directional emissivity of the surface can be written as

$$\varepsilon_{i,k}(\mu) = 1-\rho_{i,k}(\mu) \quad (i = 1,2). \tag{5}$$

Furthermore, the transmissivity of the slab surface can be written as

$$t_{i,k}(\mu) = 1-\rho_{i,k}(\mu) \quad (i = 1,2). \tag{6}$$

In expressions (5) and (6), radiative properties are considered to be dependent on the angle of incidence since from a realistic physical point of view according to Fresnel laws, reflectivity factors are angle dependent.

So, when the interfaces of the STM are to be considered with vitreous reflection, thermal boundary conditions remain the same as in the opaque case except that the term q_{si}^{*r} ($i = 1,2$) and the first term on the left-hand side of equations (3) and (4) vanish in the transparent or semi-transparent ranges, since in these regions the radiative flux is transmitted through the surface and is exchanged with $S_{-\infty}$, $S_{+\infty}$ directly; only the term q_{si}^{*r} vanishes for the opaque ranges, since there is no radiative internal flux in the opacity region.

When, in the opaque case, the Biot number at both interfaces is allowed to be very large with regard to external radiative contribution, for specified surrounding temperatures $T_{-\infty}$ and $T_{+\infty}$, the non-linear problem (2) with its modified associated boundary conditions becomes a problem with Dirichlet boundary values of prescribed temperatures or of so-called first kind boundary conditions.

If one now assumes fixed $Bi_2 = \infty$, $T_{+\infty}$ at interface S_2, and a finite value of Bi_1 at the surface S_1, one can treat the combined radiative–conductive heat transfer problem for the mixed boundary case—i.e. one face with prescribed temperature, the other submitted to given radiative and convective laws of exchange.

Therefore, by varying Biot numbers from $Bi = \infty$ to finite physical values, a single discrete formulation, equation (2), of the combined radiative–conductive transfer with general boundary conditions, equation (3), which allows the treatment, at will, for the problem of Dirichlet boundary conditions, the mixed problem or the third kind boundary conditions problem is possible.

3.3. *The radiative source term and the local radiative flux*

Determination of the discrete expression of the source term Φ_i^r in equation (2) is the central question of the coupling modelling problem in STM. From a general point of view, the source term at a control volume, say i, may be written as (Fig. 1(b))

$$\Phi_i^r = \int_{\Delta x} -\operatorname{div}\mathbf{q}^r\,dx = q_i^{r,+}(T) - q_i^{r,-}(T) = q_{i,e}^r(T) - q_{i,w}^r(T). \tag{7}$$

In this section we shall treat only the case of an STM slab fitted with its natural interfaces—i.e. of semi-transparent type with vitreous reflection—referring back to the other cases of radiative boundary conditions in the Appendix.

For such a slab of STM placed in an anisothermal situation, one can evaluate the radiative flux entering and leaving the control volume; consequently, the source term at node i becomes

$$\begin{aligned}\Phi_i^r = q_i^{r,+} - q_i^{r,-} = \sigma \sum_{k=1}^{NBA} n_{k,M}^2 \times \Bigg\{ &(V_i S_{+\infty})_{k,t\text{-}t}^s (a_{k,T_{s+\infty}} T_{s+\infty}^4 - a_{k,T_i} T_i^4) \\ &+ (V_i S_{-\infty})_{k,t\text{-}t}^s (a_{k,T_{s-\infty}} T_{s-\infty}^4 - a_{k,T_i} T_i^4) \\ &+ \sum_{j=2}^{NM-1} (V_i V_j)_{k,t\text{-}t}^s (a_{k,T_j} T_j^4 - a_{k,T_i} T_i^4) \Bigg\} \end{aligned}$$
$$(2 \leqslant i \leqslant NM-1). \tag{8}$$

If $q_i^{r,0}$ is the local radiative flux density passing through the control volume (shown in Fig. 1(b)), then the total radiative flux density crossing a surface ie situated midway between nodes i and $i+1$ can be written for semi-transparent interfaces as

$$\begin{aligned} q_{i,e}^r = q_i^{r,+} + q_i^{r,0} = \sigma \sum_{k=1}^{NBA} n_{k,M}^2 \times \Bigg\{ &\sum_{j=2}^{i} (V_j S_{+\infty})_{k,t\text{-}t}^s (a_{k,T_{s+\infty}} T_{s+\infty}^4 - a_{k,T_j} T_j^4) \\ &+ \sum_{j=i+1}^{NM-1} \sum_{l=2}^{i} (V_j V_l)_{k,t\text{-}t}^s (a_{k,T_j} T_j^4 - a_{k,T_l} T_l^4) \\ &+ \sum_{j=i+1}^{NM-1} (V_j S_{-\infty})_{k,t\text{-}t}^s (a_{k,T_j} T_j^4 - a_{k,T_{s-\infty}} T_{s-\infty}^4) \\ &+ (n_{k,rf}/n_{k,M})^2 (S_{+\infty} S_{-\infty})_{k,t\text{-}t}^s \\ &\times (a_{k,T_{s+\infty}} T_{s+\infty}^4 - a_{k,T_{s-\infty}} T_{s-\infty}^4) \Bigg\} \end{aligned}$$
$$(2 \leqslant i \leqslant NM-1). \tag{9}$$

For opaque interfaces, q_{ie}^r has already been given in ref. [15].

The local radiative flux at the surface S_1 for semi-transparent interfaces can be written as

$$\begin{aligned} q_{s1}^r = \sigma \sum_{k=1}^{NBA} n_{k,M}^2 \Bigg\{ &\sum_{j=2}^{NM-1} (V_j S_{-\infty})_{k,t\text{-}t}^s \\ &\times (a_{k,T_j} T_j^4 - a_{k,T_{s-\infty}} T_{s-\infty}^4) + (n_{k,rf}/n_{k,M})^2 (S_{+\infty} S_{-\infty})_{k,t\text{-}t}^s \\ &\times (a_{k,T_{s+\infty}} T_{s+\infty}^4 - a_{k,T_{s-\infty}} T_{s-\infty}^4) \Bigg\} \quad (i = 1) \end{aligned} \tag{10}$$

and a similar expression for the radiative flux at boundary S_2.

In expressions (8)–(10) we have introduced the symbolical writing $(S_iS_j)_k$, $(S_iV_j)_k$ and $(V_iV_j)_k$ (in Hottel and Sarofim's terminology [16] they refer to the extended exchange area (EEA) for the spectral band k) associated respectively with radiative exchanges between nodes of surface S_i and S_j, between the node of surface S_i and nodal volume V_j and finally between two nodal volumes V_i and V_j. They may have several different mathematical forms, according to the mode of reflection onto the interfaces—metallic or vitreous, specular or diffuse.

3.4. *The spectral exchange area*

When in the presence of two opaque diffusely reflecting boundaries, we have already been able to express the various spectral EEA in the framework of Gebhart's theory [17] in terms of the direct exchange area between black frontiers and radiative properties of the surfaces.

Now, we should give briefly the results of the different EEA for a slab of STM bounded by two frontiers, semi-transparent in the visible and the near-infra-red, and reflecting specularly (for semi-transparent/opaque frontiers, see ref. [18]). The two interfaces need to be smooth, so the optical path of a beam of radiation will be controlled by the laws of geometrical optics; furthermore, since the slab is plunged in a medium of lower refractive index, the transfer of energy will be subjected to the total reflection phenomenon. Figure 2 illustrates the trajectory of a single beam of radiation for such interfaces.

The model considers unpolarized radiation, but the reflectivity can be taken as the average of perpendicular and parallel components of $\rho_{i,k}(\mu)$, for which the dependence on angle of incidence may be taken into account for the various EEA calculations. The influence of such refinement will be examined in Section 4.4 only.

When the spectral transmission and reflection factors are assumed to be angle independent, the EEA between the two surrounding surfaces $S_{-\infty}$ and $S_{+\infty}$ will be, in a condensed form

$$(S_{-\infty}S_{+\infty})^{s}_{k,\mathrm{t-t}} = 2(n_{k,\mathrm{M}}/n_{k,\mathrm{rf}})^2 t^{s}_{1k} t^{s}_{2k} [F_k(\tau_{0k})]^{1}_{\mu_c} \tag{11}$$

where τ_{0k} is the spectral optical depth given by

$$\tau_{0k} = \kappa_k d \tag{12}$$

and $[F_k(z)]^1_{\mu_c}$ represents the function

$$[F_k(z)]^1_{\mu_c} = \int_{\mu_c}^{1} (\mu\, \mathrm{e}^{-z/\mu})/[1-\rho^{s}_{1k}\rho^{s}_{2k}\,\mathrm{e}^{-2\tau_{0k}/\mu}]\,\mathrm{d}\mu \tag{13}$$

with $\mu_c = \cos\theta_c = [1-(n_{\mathrm{rf}}/n_{\mathrm{M}})^2]^{1/2}$, when, according to Fig. 4, θ_c is the critical angle of reflection

The EEA between external nodes and internal surface nodes can be expressed as (allowing each emissivity for the surfaces of inner nodes to equal 1; hence the corresponding reflectivity equals zero)

$$(S_{-\infty}S_i)^{s}_{k,\mathrm{t-t}} = 2(n_{k,\mathrm{M}}/n_{k,\mathrm{rf}})^2 t^{s}_{1k}[F_k(\kappa_k x_{1,i}) + \rho^{s}_{2k}F_k(\kappa_k d + \kappa_k x_{2,i})]^1_{\mu_c} \tag{14}$$

where the function $[F_k(z)]^1_{\mu_c}$ has been previously defined in equation (14), and $x_{1,i}$, $x_{2,i}$ designate, respectively, the distance of separation between interface S_1 and node i and that between interface S_2 and node i. The principle of energy conservation leads to

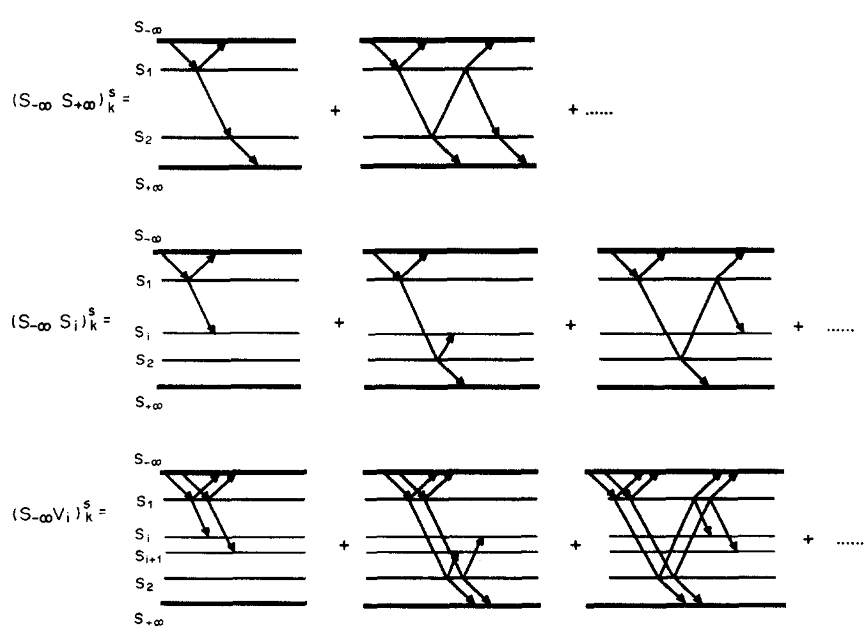

FIG. 2. Diagram showing, by the ray tracing method, the formation of an extended exchange area for semi-transparent frontiers.

a relationship linking EEA between a surface and a volume and EEA between two surfaces

$$n_{k,\mathrm{rf}}^2(S_{-\infty}V_i)_{k,\mathrm{t\text{-}t}}^{\mathrm{s}} = 2n_{k,\mathrm{M}}^2 t_{1k}^{\mathrm{s}}[F_k(\kappa_k x_{1,i}) - F_k(\kappa_k x_{1,i+1}) + \rho_{2k}^{\mathrm{s}} F_k(\kappa_k d + \kappa_k x_{2,i+1}) - \rho_{2k}^{\mathrm{s}} F_k(\kappa_k d + \kappa_k x_{2,i})]_{\mu_c}^1. \quad (15)$$

In fact, radiation coming from $S_{-\infty}$ and transmitted across interface S_1 is either absorbed by the volume node V_i by crossing internal surface S_i or escapes from the surface S_{i+1}. The corresponding expression for $(S_{+\infty}V_i)_{k,\mathrm{t\text{-}t}}^{\mathrm{s}}$ is

$$n_{k,\mathrm{rf}}^2(S_{+\infty}V_i)_{k,\mathrm{t\text{-}t}}^{\mathrm{s}} = 2n_{k,\mathrm{M}}^2 t_{2k}^{\mathrm{s}}[F_k(\kappa_k x_{i+1,2}) - F_k(\kappa_k x_{i,2}) + \rho_{1k}^{\mathrm{s}} F_k(\kappa_k x_{i,1} + \kappa_k d) - \rho_{1k}^{\mathrm{s}} F_k(\kappa_k x_{i+1,1} + \kappa_k d)]_{\mu_c}^1. \quad (16)$$

Radiative interchange processes between internodal surfaces S_i and S_j by taking into account multiple reflections onto external surfaces lead to the corresponding EEA

$$\begin{aligned}(S_iS_j)_{k,\mathrm{t\text{-}t}}^{\mathrm{s}} = 2\{&[F_k(\kappa_k x_{ij}) + F_k(\kappa_k x_{i,2} + \kappa_k x_{2,j}) \\ &+ F_k(\kappa_k x_{i,1} + \kappa_k x_{1,j}) + F_k(\kappa_k x_{i,1} + \kappa_k d + \kappa_k x_{2,j})]_0^{\mu_c} \\ &+ [F_k(\kappa_k x_{i,j}) + \rho_{2k}^{\mathrm{s}} F_k(\kappa_k x_{i,2} + \kappa_k x_{2,j}) \\ &+ \rho_{1k}^{\mathrm{s}} F_k(\kappa_k x_{i,1} + \kappa_k x_{1,j}) \\ &+ \rho_{1k}^{\mathrm{s}}\rho_{2k}^{\mathrm{s}} F_k(\kappa_k x_{i,1} + \kappa_k d + \kappa_k x_{2,j})]_{\mu_c}^1\}. \quad (17)\end{aligned}$$

Here, we consider

$$[F_k(z)]_0^{\mu_c} = \int_0^{\mu_c} (\mu\, \mathrm{e}^{-z/\mu})/[1-\mathrm{e}^{-2\tau_{0k}/\mu}]\,\mathrm{d}\mu$$

$$[F_k(z)]_{\mu_c}^1 = \int_{\mu_c}^1 (\mu\, \mathrm{e}^{-z/\mu})/[1-\rho_{1k}^{\mathrm{s}}\rho_{2k}^{\mathrm{s}}\, \mathrm{e}^{-2\tau_{0k}/\mu}]\,\mathrm{d}\mu. \quad (18)$$

Invoking again the principle of energy conservation, we have the extended exchange area between two internal nodes of volume

$$\begin{aligned}(V_iV_j)_{k,\mathrm{t\text{-}t}}^{\mathrm{s}} = 2\{&[F_k(\kappa_k x_{i+1,j}) - F_k(\kappa_k x_{i+1,j+1}) \\ &- F_k(\kappa_k x_{ij}) + F_k(\kappa_k x_{i,j+1})]_0^{\mu_c} \\ &+ [F_k(\kappa_k x_{i+1,2} + \kappa_k x_{2,j+1}) - F_k(\kappa_k x_{i+1,2} + \kappa_k x_{2,j}) \\ &- F_k(\kappa_k x_{i,2} + \kappa_k x_{2,j+1}) + F_k(\kappa_k x_{i,2} + \kappa_k x_{2,j})]_0^{\mu_c} \\ &+ [F_k(\kappa_k x_{i,1} + \kappa_k x_{1,j}) - F_k(\kappa_k x_{i,1} + \kappa_k x_{1,j+1}) \\ &- F_k(\kappa_k x_{i+1,1} + \kappa_k x_{1,j}) + F_k(\kappa_k x_{i+1,1} + \kappa_k x_{1,j+1})]_0^{\mu_c} \\ &+ [F_k(\kappa_k x_{i,1} + \kappa_k d + \kappa_k x_{2,j+1}) - F_k(\kappa_k x_{i,1} \\ &+ \kappa_k d + \kappa_k x_{2,j}) - F_k(\kappa_k x_{i+1,1} + \kappa_k d + \kappa_k x_{2,j+1}) \\ &+ F_k(\kappa_k x_{i+1,1} + \kappa_k d + \kappa_k x_{2,j})]_0^{\mu_c} \\ &+ [F_k(\kappa_k x_{i+1,j}) - F_k(\kappa_k x_{i+1,j+1}) - F_k(\kappa_k x_{i,j}) \\ &+ F_k(\kappa_k x_{i,j+1})]_{\mu_c}^1 + \rho_{2k}^{\mathrm{s}}[F_k(\kappa_k x_{i+1,2} \\ &+ \kappa_k x_{2,j+1}) - F_k(\kappa_k x_{i+1,2} + \kappa_k x_{2,j}) \\ &- F_k(\kappa_k x_{i,2} + \kappa_k x_{2,j+1}) + F_k(\kappa_k x_{i,2} + \kappa_k x_{2,j})]_{\mu_c}^1 \\ &+ \rho_{1k}^{\mathrm{s}}[F_k(\kappa_k x_{i,1} + \kappa_k x_{1,j}) - F_k(\kappa_k x_{i,1} + \kappa_k x_{1,j+1}) \\ &- F_k(\kappa_k x_{i+1,1} + \kappa_k x_{1,j}) + F_k(\kappa_k x_{i+1,1} \\ &+ \kappa_k x_{1,j+1})]_{\mu_c}^1 + \rho_{1k}^{\mathrm{s}}\rho_{2k}^{\mathrm{s}}[F_k(\kappa_k x_{i,1} \\ &+ \kappa_k d + \kappa_k x_{2,j+1}) - F_k(\kappa_k x_{i,1} + \kappa_k d + \kappa_k x_{2,j}) \\ &- F_k(\kappa_k x_{i+1,1} + \kappa_k d + \kappa_k x_{2,j+1}) \\ &+ F_k(\kappa_k x_{i+1,1} + \kappa_k d + \kappa_k x_{2,j})]_{\mu_c}^1\}. \quad (19)\end{aligned}$$

Furthermore, the extended reciprocity relation can be written as

$$\begin{aligned}(S_{-\infty}S_{+\infty})_{k,\mathrm{t\text{-}t}}^{\mathrm{s}} &= (S_{+\infty}S_{-\infty})_{k,\mathrm{t\text{-}t}}^{\mathrm{s}}, \\ n_{k,\mathrm{rf}}^2(S_{-\infty}V_i)_{k,\mathrm{t\text{-}t}}^{\mathrm{s}} &= n_{k,\mathrm{M}}^2(V_iS_{-\infty})_{k,\mathrm{t\text{-}t}}^{\mathrm{s}} \\ (V_iV_j)_{k,\mathrm{t\text{-}t}}^{\mathrm{s}} &= (V_jV_i)_{k,\mathrm{t\text{-}t}}^{\mathrm{s}}, \\ n_{k,\mathrm{rf}}^2(S_{+\infty}V_i)_{k,\mathrm{t\text{-}t}}^{\mathrm{s}} &= n_{k,\mathrm{M}}^2(V_iS_{+\infty})_{k,\mathrm{t\text{-}t}}^{\mathrm{s}}. \quad (20)\end{aligned}$$

3.5. *The numerical treatment*

The source terms given by equation (8) are nonlinear functions of T; in order to include them in the numerical scheme, the general expression has been transformed in a more tractable form by following Patankar's method [19]. It consists of separating, by introducing a supplementary iterative step, say n, the given source term into a constant part, Sc, which is calculated at time step $m+1$ and iteration n, and a linear temperature-dependent part at node i for the instant $m+1$. So one can write for the source term

$$\Phi_i^{\mathrm{r},m+1,n+1} = Sc_i^{m+1,n+1} + Sp_i^{m+1,n+1}T_i^{m+1,n+1} \quad (21)$$

with Sp always negative to ensure the stability of the numerical process.

The solution is assumed to converge at each time step, m, when, for each node, the difference in temperatures between two iterations n and $n+1$ satisfies

$$|T_i^{m,n+1} - T_i^{m,n}| < 0.001\ \mathrm{K}. \quad (22)$$

A variable time step Δt^*, which gradually increases according to the relation [9]

$$\Delta t^* = 1.0 - \exp(-\gamma m) \quad (23)$$

is used in most computations unless otherwise specified. Here, m is a time step counter and $\gamma = 2.23\times10^{-5}$ controls the rate of increase of Δt^*. The field of temperature is assumed to be stabilized when the difference of the temperatures between two time steps m and $m+1$ satisfies

$$|T_i^{m+1,nf} - T_i^{m,nf}| < 0.001\ \mathrm{K} \quad (24)$$

at each node. Here, the superscript nf designates the final iterative solution.

In all calculations, the convergence of the solution with respect to the grid size is also assured. The node number NM was chosen until the total heat flux reached a constant value (since the total heat flux is more sensitive than temperature). For example, $NM = 50$ for a 1 cm slab, with spectrum A (see Table 1), $T_{s1} = 750$ K and $T_{s2} = 1500$ K; and $NM = 70$ for a 10 cm slab, the other parameters remaining the same.

4. TRANSIENT HEAT TRANSFER FOR AN OPAQUE BOUNDARY AND SPECIFIED BOUNDARY TEMPERATURE

It is assumed that initially the STM wall is fitted with opaque frontiers and stands at uniform temperature T_{s2}; one of its boundaries is suddenly held at the fixed temperature T_{s1}, up to the steady state. The following results have been computed for the temperature conditions: $T_{rf1} = T_{s1} = 750$ K and $T_{rf2} = T_{s2} = 1500$ K. So we have to solve the problem for boundary conditions (3) by setting

$$Bi_1 = Bi_2 = \infty$$

$$T^*_{-\infty}(t) = 0.5; \quad T^*_{+\infty}(t) = 1 \tag{25}$$

with the initial condition

$$T^*(\xi, t = 0) = 1 \quad (0 \leqslant \xi \leqslant 1). \tag{26}$$

Resolution of the numerical problem by an implicit scheme provides the inner field temperature of the STM slab for various Fourier numbers (or dimensionless times). Afterwards, in order to calculate the radiative heat flux, these data are incorporated into the nodal discrete expression (9).

4.1. *Influence of the coupling parameter* N_P

Temperature and flux profiles of an STM wall of absorption spectrum A, bounded by black frontiers, are shown in Figs. 3(a)–(c) for dimensionless time $t^*(d)$ (or Fourier numbers $Fo(d)$) and conductive–radiative coupling parameters $N_P = 0.5$, 0.05 and 0.005 (corresponding to a thickness of 1 cm) [20].

The principal trends of the combined transfer described earlier by Doornink and Hering [3], as well as by Lauriat [5] for the grey wall case, are recovered. One can summarize them as follows.

(1) For small dimensionless times, thermal gradients are elevated in the vicinity of the cooled boundary and the conduction phenomenon is dominant. For a given infra-red spectrum, the transferred radiative flux participates little by comparison with the conductive one. Profiles of radiative flux display a maximum which appears near the cooled part of the slab, showing a radiative heating of the cooled part of the slab and a radiative cooling of its major inner part.

(2) At intermediate dimensionless times, i.e. long before the steady state, the coupling produces a drastic cooling of the zone—never influenced by the hot boundary—and all the more so as N_P is weak; for example, if $N_P = 0.005$, a heat sink appears near the hot interface which loses more energy by radiation than it gains. The position of the radiative flux maximum moves towards the hot surface, indicating an expansion of the radiatively heated zone.

(3) In STM absorption of radiation at a distance increases when N_P decreases and consequently the mean temperature gets higher; thus the reduced times needed to reach the steady state are shortened. Reduced times (and associated physical times) satisfying criterion (24) are reported in Table 2 and may be compared with the corresponding time needed to set up the purely conductive transfer steady state.

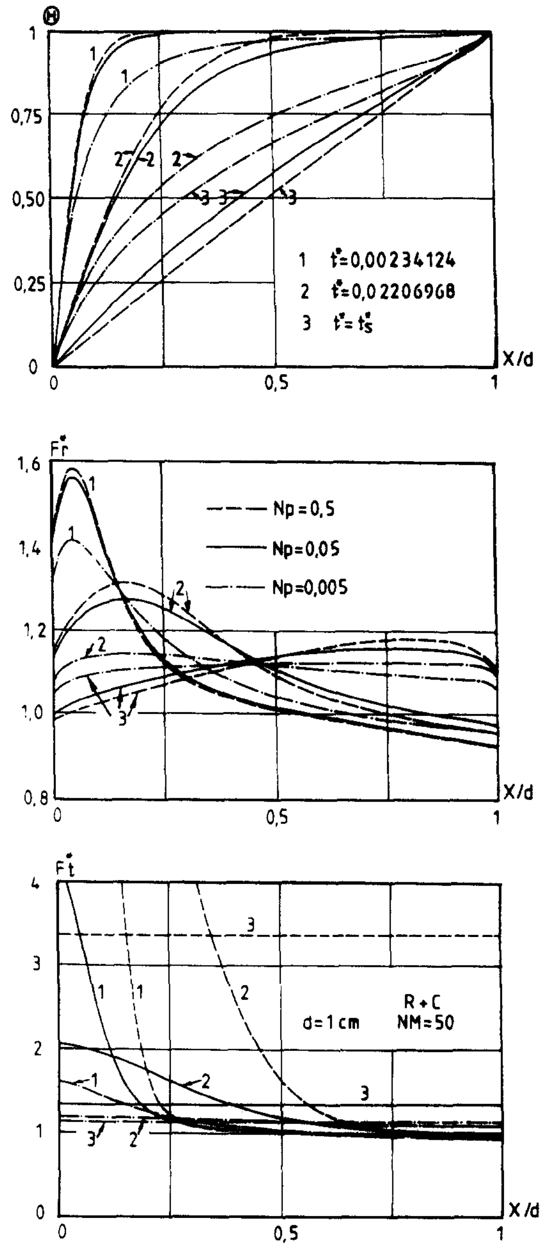

FIG. 3. Temperature, radiative and total flux profiles in non-grey glasses of thickness $d = 1$ cm, subjected to fixed temperature conditions, for various Planck numbers $N_P = 0.5, 0.05, 0.005$.

In the steady state, thermal gradients increase near the boundaries, involving higher conductive exchanges, leading to the well-known S-shape temperature profiles of the simultaneous radiative–conductive heat transfer. When N_P is very small, heat transfer is carried out almost purely by radiation, and temperature profiles are close to the discontinuous distribution characterized by the slipping effect.

Table 2. Reduced and physical times needed to reach the steady state

N_P	Spectrum A	Spectrum B	Conduction
0.500	1.035 (10.35 s)	1.004 (10.05 s)	1.0794 (10.79 s)
0.050	0.7322 (73.22 s)	0.6121 (61.21 s)	1.0794 (107.9 s)
0.005	0.2168 (216.8 s)	0.1435 (143.5 s)	1.0794 (1079 s)

4.2. *Influence of the absorption spectrum shape*

In the transient situations, results of the examination of the absorption spectra shape modification (spectra A and B), reported below, concern a slab of 10 cm thickness ($N_P = 0.005$) bounded by black coating and are represented in Fig. 4. One can note the following points.

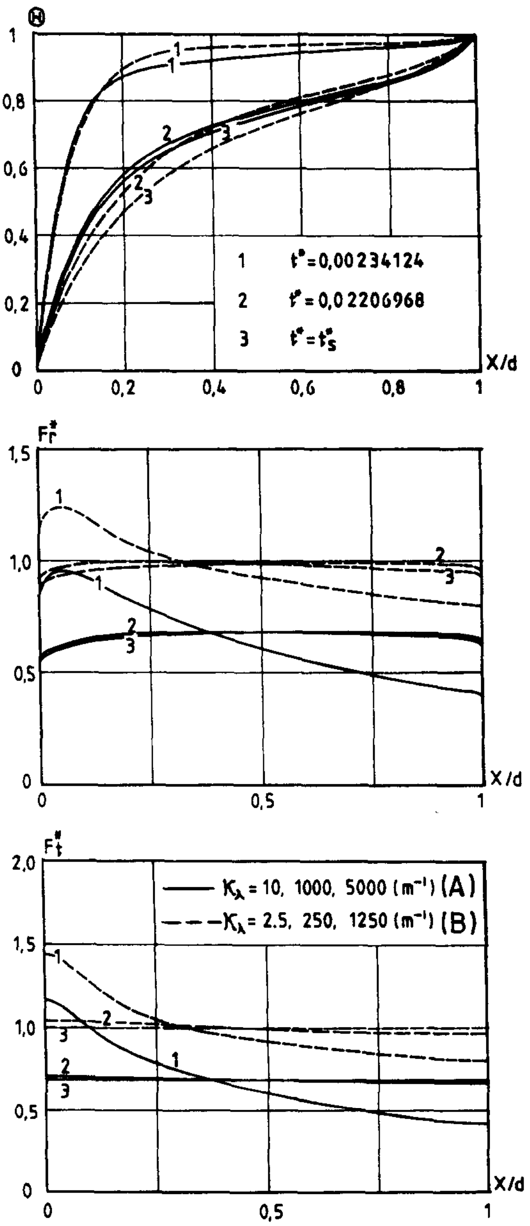

FIG. 4. Effect of spectrum shape on temperature, radiative and total flux profiles (spectra A and B), $d = 10$ cm.

(1) At early reduced times, there is some difference in temperature profiles for the two materials in the hot part of the layer. Isochrones for spectrum A decrease at a faster rate than those for spectrum B.

(2) As already mentioned, flux density profiles are more sensitive quantities. One may observe, in Fig. 4, differences at small times between radiative transfer importance for spectra A and B in favour of the most transparent material.

(3) When numerical modelling is carried out for higher thicknesses, these trends are enhanced.

4.3. *Effect of a change in the radiative properties of the boundaries*

The effects of a change in the radiative characteristics of the frontiers on the flux profiles, involving passing from a system with two black boundaries to almost fully reflecting ones, are shown in Fig. 5 for a 1 cm thick non-grey material of spectrum A, leading to the following observations: although temperature distributions are not strongly modified for that thickness ($N_P = 0.05$), on radiative flux profiles there occurs a very important decrease in the radiative heat flux magnitude—by a factor of three at the maximum for small times—due to less effective cooling and heating at a distance. At the two slab extremities the radiative flux tends towards zero since the net radiative flux (leaving flux minus incident flux) goes to a null value as the emissivities of the frontiers vanish. So, when multiple reflections are taken into account, total heat fluxes are correspondingly weaker than in the black case.

So far, the various effective exchange areas entering into the radiative source term have been computed for the diffuse reflection case, but they may be obtained also for the specular reflection model. For a grey slab of STM of optical thickness $\tau_0 = 1$, submitted to first kind thermal boundary conditions, differences of a few thousandths of a degree in the two calculated profiles have been observed for specified temperatures $T_{-\infty} = 100$ K and $T_{+\infty} = 1000$ K when the emissivities of the frontiers are $\varepsilon_1 = \varepsilon_2 = 0.1$, in agreement with Anderson and Viskanta's results [21].

4.4. *Effect of angular dependence of radiative properties of the boundaries*

The influence of the angular dependence of the mean spectral reflectivity

$$\bar{\rho}_k(\mu) = 1/2[\rho_{k\parallel}(\mu) + \rho_{k\perp}(\mu)] \tag{27}$$

has also been examined for a flat layer of STM bounded by an opaque metallic coating. The direc-

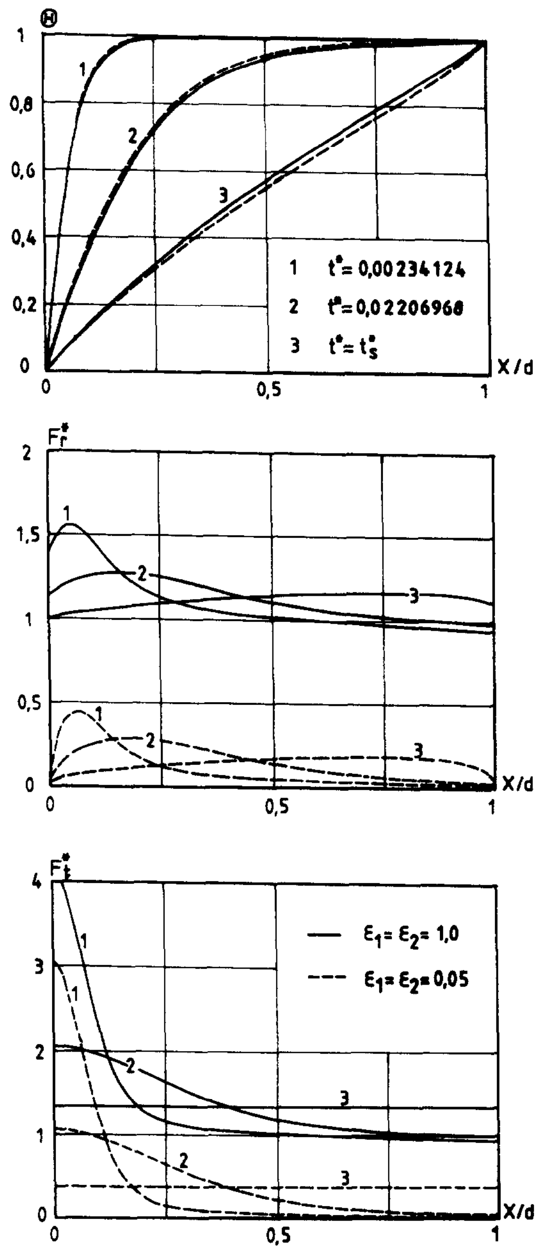

FIG. 5. Effect of a change in radiative properties, for a slab of $d = 1$ cm, for fixed boundary temperatures.

tional spectral reflectivity has been calculated by means of Fresnel's equations, where a complex index of refraction of the metal was introduced [16] and all EEAs corresponding to modified equations (11)–(20) have been re-evaluated by means of a supplementary angle discretization.

Temperature profiles for the first kind of thermal boundary conditions obtained with angle-dependent radiative properties, by comparison with results for angular independence, have shown very little effect (only 0.3 K at 1000 K) for a 1 cm thick slab of spectrum A coated with platinum. This result justifies neglecting radiative directional properties for opaque dielectric–conductor interfaces, but cannot be generalized to interfaces between two dielectric media. In fact, spectral transmission and reflection (equations (5) and (6)) of the layer boundaries are dependent on the $\rho_{\parallel k}(\mu)$ and $\rho_{\perp k}(\mu)$ polarization components, since, if internal primary thermal radiation beams are unpolarized, they become partly polarized upon reflections according to incident angle; furthermore, multiple reflections between parallel interfaces increase the degree of polarization.

Polarization effects have to be expected near the Brewster angle and in the vicinity of the grazing angle; accordingly they would be more important in thin media than in large optical thicknesses. However, in the following they have been ignored.

5. TRANSIENT HEAT TRANSFER IN THE MIXED BOUNDARY CONDITION CASE

Modelling by the nodal analysis is now used to solve more complex radiative–conductive heat transfer problems—those of a plane layer of an STM the temperature of which is prescribed on one interface, the opposite face being subjected to radiative–convective heat exchanges. Two examples will be treated by varying the fixed temperature.

In the first example, the prescribed temperature is the initial one, $T_{+\infty} = T_{rf2} = 1500$ K; on the other face the slab can exchange with the environment, the temperature of which is $T_{-\infty} = T_{rf1} = 750$ K, by both radiative cooling and natural convection controlled by several Biot numbers values varying between 0.1 and ∞ (Fig. 6). The layer is a 10 cm (corresponding to $N_P = 0.005$, $\lambda = 0.86113$ W m^{-1} K^{-1}) thick slab of 'float' glass of spectrum A. The hot face is opaque and coated with a reflecting layer ($\rho_{2k} = 0.97$); for the other face, two radiative boundary conditions are selected—it is either transparent (transmissivity $\tau_k = 0.96$ for transparent and semi-transparent regions, and emissivity $\varepsilon_k = 0.94$ for opaque region) or opaque (emissivity $\varepsilon_k = 0.94$–0.96).

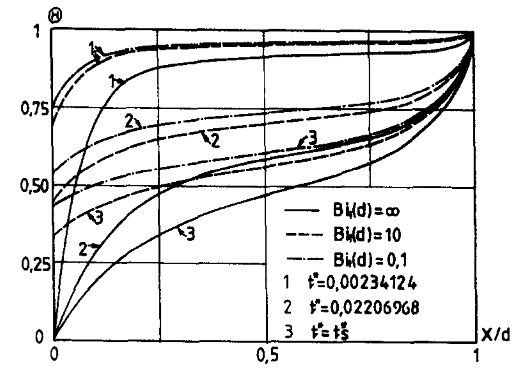

FIG. 6. Temperature profiles at various times with mixed conditions for various Biot numbers.

So, the solution of this problem is achieved by making use of equation (2) with boundary conditions (3)

$$Bi_1 = \infty, \quad T^*_{+\infty} = 1, \quad T^*_{-\infty} = 0.5 \qquad (28)$$

with the initial condition

$$T^*(\xi, t = 0) = 1. \qquad (29)$$

The transient and the permanent temperature profiles are plotted in Fig. 6 in the case of the two opaque frontiers. When convective exchanges are poor, the temperature setting up for the cold face is much higher than the environmental one. With more effective convective dissipation, the different isochrones move towards lower temperatures. For direct perfect contact between the cooled face and the ambient medium, the resulting temperature profile is of the same kind as that discussed in relation to Fig. 3(c) (but thermal conductivity and emissivities have been chosen different). In the steady state, the low temperature gradient at the free interface in the presence of small convective effects can be noticed.

For the radiative heat flux, if their profiles are very different at small times, in the steady state they are very close and uniform, except in the hot zone near the reflecting frontier.

Results for the same STM fitted with semi-transparent natural frontier on the free side of the layer ($Bi = 0.1$), are illustrated in Fig. 7 and compared with the previous calculations for two opaque frontiers.

As a second example, the prescribed temperature is half of the initial one, i.e. $T_{+\infty} = T_{rf2} = 750$ K. Thermal boundary conditions are therefore similar to the above, except that $T^*_{+\infty} = 0.5$. The chosen radiative conditions are those of a slab limited by an isothermal opaque frontier, determined by a metallic bath of low emissivity and, on the opposite side, by a semi-transparent interface with vitreous reflections. It can be representative of a rough simulation of glass-making by the float process.

The evolution of the temperature distribution within the glass sheet is displayed in Fig. 8 for five

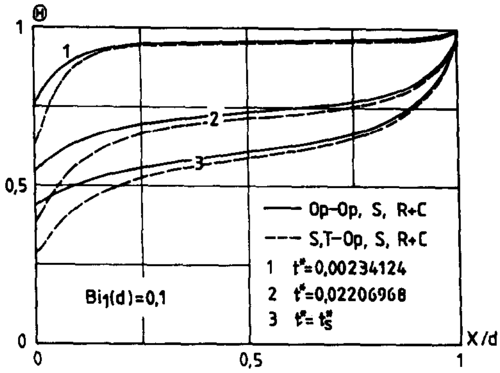

FIG. 7. Temperature profiles for mixed conditions: $T_{s1} = T_{\text{initial}}$. Comparison for opaque/opaque and semi-transparent/opaque frontiers.

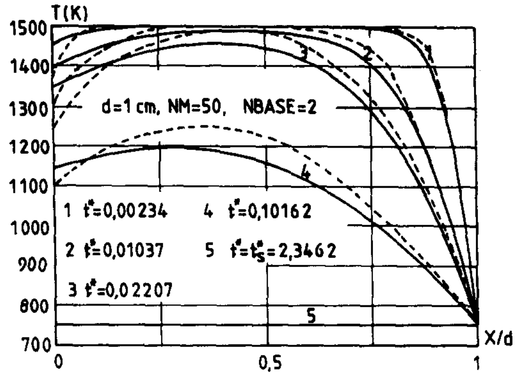

FIG. 8. Temperature profiles for mixed kind conditions, for a sudden drop of temperature T_{s1}, $d = 1$ cm (spectrum A), for opaque/semi-transparent frontiers. ---, Comparison with pure conductive exchanges.

different times of the cooling process. At early times, the region of the STM slab in direct contact with the metallic bath loses its energy by conduction only, by thermal mechanisms already described in Section 4, although the free interface is cooled by convection; the central part of the layer, still at a high temperature, exchanges heat by radiation with the cold parts. As a result, the mean temperature is decreasing, as is the gradient magnitude. At very long times, the temperature of the slab becomes uniform except near the zone which is still under the influence of the cold frontier. Also in Fig. 8 a comparison is made with the pure conductive case.

6. TRANSIENT TRANSFER WITH IMPOSED EXCHANGE BOUNDARY CONDITIONS (SYMMETRICAL CASE)

Let us now consider the problem of the return to thermal equilibrium of a plane parallel STM slab which initially stands at a high uniform temperature and is submitted to internal combined radiative–conductive heat transfer and to external simultaneous convective and radiative exchanges at its two boundaries.

Mathematically, the problem has its full non-linearity features both in the governing local equation and in radiative boundary conditions. It depends on the influence of the different free parameters, Planck number N_P, Biot number Bi and Fourier number Fo; it would depend also on the two kinds of emissivity condition at the interfaces.

6.1. *Analysis of the results for the combined problem (symmetrical case)*

The combined problem is worked out by making use of the discretized radiative–conductive equation (2) associated with the fairly general radiative–convective boundary conditions (3).

The considered medium is still a typical glass of thickness 0.5 cm, the near-infra-red absorption spectrum of which is of C type (refer to Table 1). The radiative interchange with external surroundings is determined either by the mid-infra-red properties of the interface, described by a two-band rectangular model for vitreous reflection, or by the complete multi-band infra-red spectrum, in the case of an opaque boundary. Frontiers are assumed to reflect radiations according to geometrical optic concepts, i.e. following reflection and refraction laws at the interface; in particular, for vitreous reflection, a transmitted radiation pencil is subject to the total reflection phenomenon.

Calculations were carried out for an inner initial temperature $T_0 = T_{rf2} = 1500$ K and an ambient temperature, $T_{\pm\infty} = T_{rf1} = 750$ K.

6.1.1. *Effect of the radiative–conductive coupling parameter* N_P. In this section, the Planck number is always defined in terms of the initial uniform temperature of the slab, T_0. Since the proportions of radiative and conductive modes vary with time, it has no constant signification, but is used as a classifier. Its values are calculated by changing the thermal conductivity of the layer.

(1) Opaque boundaries. The evolution of the temperature distribution during the cooling phase of the STM slab fitted with opaque boundaries (curves R+C) is represented in Figs. 9(a)–(c) for $Bi = 0.05$ and various values of the internal coupling parameter N_P between 0.05 and 0.0005. They are compared (curves C) with results obtained for a fully opaque medium, all things being equal from the thermal point of view.

For the symmetrical exchange case, on the temperature profiles at small and intermediate times one can observe, roughly, the existence of two thermal regions, one situated in the central part with low variations, the other with high thermal gradients near the boundary (the thermal layer). Comparison of the various isochrones R+C and C displays a faster cooling rate of the central part when there is radiative participation and a flatter isothermal profile, as well as reduced thermal gradients. At very small Planck numbers ($N_P = 0.0005$), the separation between isochrone curves R+C and C becomes particularly evident, the acceleration of heat exchanges involves a considerable decrease in the mean temperature, and different time scales of exchange phenomena appear. The thickness of the thermal layer decreases and the rate of cooling goes on increasing. Moreover, radiative heating at a distance erases frontier gradients due to conduction and as a result very uniform temperature profiles are set up at long reduced times for the long times.

By focusing on flux profiles, one can notice again that, at small Fourier numbers, the main contribution to the transfer is due to the conduction mode allowing communication of the energy between the interior

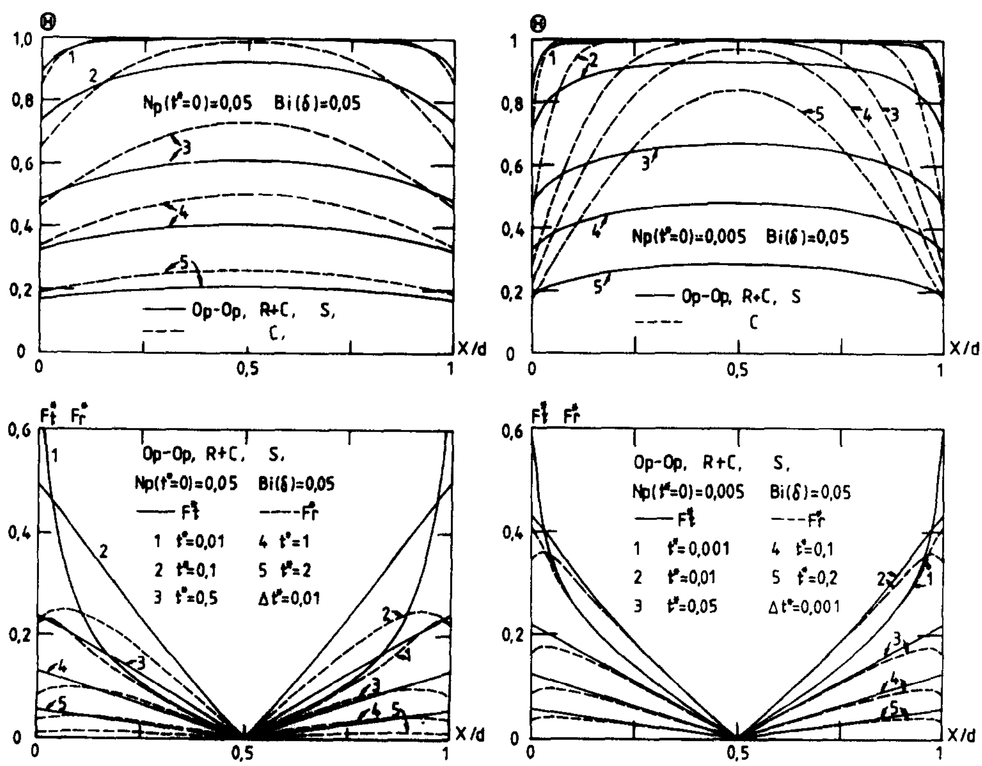

FIG. 9. Temperature and flux profiles for heat exchange (symmetrical) conditions, $N_P = 0.05$, 0.005 and 0.0005. Comparison for the opaque/opaque case between combined (R+C) and pure conductive (C) transfers.

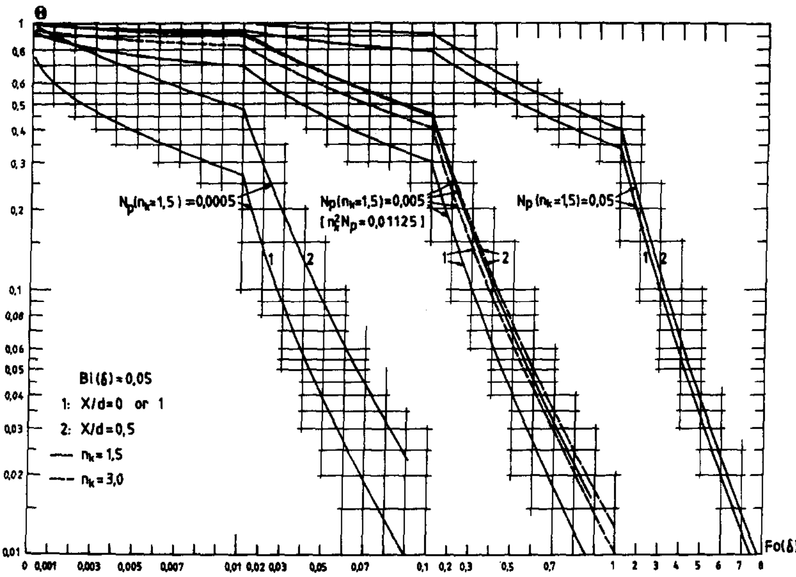

FIG. 10. Diagram of reduced temperature vs Fourier number for various N_P and refractive index values: (1) surface temperature; (2) central temperature.

and the exterior of the wall. For rather long times ($Fo(\delta) = 0.1$) conductive transfer is significant within the wall, for thermal gradients are increasing, the total heat transfer improves and tends to become linear as soon as $Fo(\delta) = 0.5$. As time passes, the mean temperature of the slab decreases and the two transferred fluxes get weaker until thermal equilibrium is reached.

Like combined transfer with prescribed temperatures, examination of the radiative flux distribution shows the existence of a maximum in the proximity of the boundaries at small *Fo*, which indicates excess of absorption over emission in the thermal layer.

(2) Semi-transparent interfaces. When semi-transparent interfaces are present the previous trends—flatter temperature profiles, slight increase of the cooling rate—are preserved.

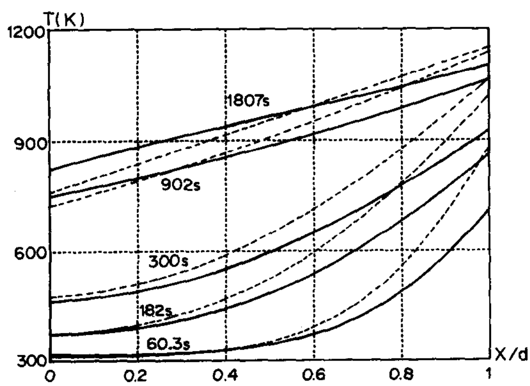

FIG. 11. Temperature profiles for a windshield during re-entry. Temperature of the flow: 1200 K. Full line, semi-transparent frontiers. Dashed line, pure conductive exchanges.

Figure 10 represents, in semi-log coordinates, the evolution of the surface ($\xi = 0$ or 1) and the central ($\xi = 0.5$) reduced temperature against Fourier number of an STM slab with semi-transparent interfaces for various values of the ratio $1/N_P$ and a given small Biot number. The resulting curve network appears to be very similar to the classical diagram of the pure conductive theory when defined in terms of the same pair of variables, with the Planck number replacing the Biot number here. This fact leads to the conclusion that for combined radiative–conductive transfer in STM, the ratio $1/N_P$ plays the same role as *Bi* for the convective exchanges alone. In Fig. 10 it is also seen that cooling processes take place for Fourier numbers varying roughly inversely with Planck number when the steady state is approached.

Construction of such a generalized abacus for given Biot numbers and various Planck numbers makes it possible to provide quick predictions of the temperature evolution of flat glasses with known optical properties.

6.1.2. *Sensitivity against the refractive index.* Also plotted in Fig. 10 is the evolution of the nodal and central temperature against Fourier numbers, calculated for two distinct refractive index values, $n = 1.5$ and 3. Since the interfaces of the wall are assumed to be transparent with vitreous reflections, a change of the refractive index involves several modifications of radiative transfers due to variations of reflection (according to Fresnel laws), transmission factors, variation of the limited reflection angle and expression of the radiative flux density itself, as seen by inspection of equation (10). It is noticed that modelling of a 0.5 cm thick slab does not bring about many changes in the diagram $(\Theta, Fo(\delta))$ for a given set of values of $n^2 N_P$ and Bi. For the particular case studied, by passing from $n = 1.5$ to 3, one can observe an increase in the temperature of the surface node for small Fourier numbers, but no variation of central temperature up to $Fo = 0.1$.

7. TRANSIENT COUPLED HEAT TRANSFER FOR ASYMMETRICAL EXCHANGES

We now consider a plane parallel wall of STM which is assumed to be cooled on one of its sides by simultaneous natural convection and radiative exchanges and heated on the opposite side by a gaseous hot flow, characterized by a forced convective heat exchange coefficient and a black body temperature $T_{+\infty}$. This example is related to the important aerothermal problem of the thermal behaviour description of a spacecraft engine windshield during re-entry into the terrestrial atmosphere.

Realistic geometrical and physical conditions are taken into account, but ablation phenomena are neglected. The STM window will be a 3 cm thick slab of fused silica, the absorption spectrum, refractive index and emissivity (angular dependent) of which in the infra-red are modelled by six rectangular bands, as reported in Table 3.

Thermal boundary conditions adjacent to the window are: initial temperature $T_0 = 311$ K, internal heat exchange coefficient corresponding to the natural convection process set up in the cabin $h_1 = 10$ W m^{-2} K^{-1}, external exchange coefficient $h_2 = 100$ W m^{-2} K^{-1}, gas emissivity $\varepsilon_{\pm\infty} = 1$. The value of the external gas temperature (assumed to be constant during the flight) has been chosen as that of a conventional re-entry: $T_{+\infty} = 1200$ K.

Temperature profiles predicted by the one-dimensional modelling of the transient combined heat transfer for the spacecraft window exposed to external convective and radiating heating are illustrated in Fig. 11 in the time interval determined from the beginning of the heating process up to 30 min later.

As shown on this graph, the temperature of the outer face rises quickly in the first few moments, reaching 711 K after only 60 s, whereas the inner face temperature increases at a lower rate. In this case, the temperature of the hot face becomes 1102 K, with a temperature difference of only 279 K between the two faces, when 30 min have passed, and stays quite a long way below the working temperature of the vitreous silica (1900–2000 K). Also shown in Fig. 11 are predictions of temperature profiles for a purely conducting flat layer of the same thermal conductivity as the STM.

In order to prevent radiative heating in the cabin, the windshield may be re-covered by a reflecting metallic coating on the inner face. In these circumstances the model shows that the temperature of the hot frontier is not modified; however, the internal face temperature and the inner temperature of the slab are significantly modified—they quickly reach a high level uniform temperature distribution due to the absorption of the reflected flux near the rear interface.

Table 3. Optical characteristics of fused silica used

λ (μm)	κ_λ (cm^{-1})	n	ρ_1	ρ_2
0.40–2.65	1	1.45	0.03 or 1.0	0.03
2.65–2.90	1000	1.434	0.03 or 1.0	0.03
2.90–4.20	5	1.42	0.03 or 1.0	0.03
4.20–7.00	5000	1.35	0.05 or 1.0	0.05
7.00–11.0	5000	1.30	0.50 or 1.0	0.50
11.0–20.0	5000	1.30	0.07 or 1.0	0.07

8. CONCLUSION

In the framework of the nodal analysis and Hottel's zonal method, extended by the ray tracing method, the thermal behaviour of an STM submitted to fairly general radiative and thermal boundary conditions can be predicted. The method brings together and makes use of, in the one-dimensional geometry, the set of macroscopic physical laws (optical and thermal) which govern the combined heat transfers in an STM, from an internal coupling point of view as well as from exchanges with the environment through interfaces.

The single algorithm presented here, which has been developed taking full account of the non-linearity features of the problem, can be used to obtain predictions of temperature and heat flux profiles within an STM slab for realistic absorption infra-red spectra and various thermal non-equilibrium situations of physical and technological interest. The few examples treated point to the adaptability of the method and could be multiplied at will by changing parameters such as radiative properties of the layer and the algebraic sign and magnitude of convective heat exchange processes, as well as the initial internal temperature conditions and exchange temperature of the environment.

REFERENCES

1. R. Viskanta and E. E. Anderson, Heat transfer in semi-transparent solids. In *Advances in Heat Transfer*, Vol. 11, pp. 317–441. Academic Press, New York (1975).
2. G. K. Chui and R. Gardon, Interaction of radiation and conduction in glass, *J. Am. Ceram. Soc.* **52,** 548–553 (1969).
3. D. G. Doornink and R. G. Hering, Transient combined conductive and radiative heat transfer, *J. Heat Transfer* **94,** 473–478 (1972).
4. K. C. Weston and J. L. Hauth, Unsteady, combined radiation and conduction in an absorbing, scattering and emitting medium, *J. Heat Transfer* **95,** 357–364 (1973).
5. G. Lauriat, Contribution à l'étude du transfert de chaleur dans les milieux semi-transparents, Thèse de Docteur de troisième cycle, Paris (1974).
6. J. B. Saulnier, La modélisation thermique et ses applications aux transferts couplés et au contrôle actif, Thèse de Doctorat d'Etat, Université de Poitiers (1980).
7. W. H. Sutton, A short time solution for coupled con-

duction and radiation in a participating slab geometry, *J. Heat Transfer* **108**, 465–466 (1986).
8. D. E. Glass, M. N. Özisik and D. S. McRae, Combined conduction and radiation with flux boundary condition for a semi-transparent medium covered by thin radiating layers, *J. Quant. Spectrosc. Radiat. Transfer* **38**(3), 201–208 (1987).
9. V. K. Bityukov, V. A. Petrov and S. V. Stephanov, Contactless measurement of the thermal conductivity of semi-transparent materials at high temperatures, *High Temp.–High Pressures* **12**, 229–236 (1980).
10. R. Viskanta and D. M. Kim, Heat transfer through irradiated semi-transparent layers at high temperature, *J. Heat Transfer* **102**, 182–184 (1980).
11. D. Ramerth and R. Viskanta, Heat transfer through semi-transparent coal-ash deposits, contributed by the Heat Transfer Division of the ASME, 82-HT-2 (1982).
12. M. Kuriyama, K. Katayama, Y. Takuma, Y. Hasegawa and T. Ohsaka, Analytical study of radiation and conduction heat transfer in infrared transmitting chalcogenide glass, *Bull. J.S.M.E.* **18**(124), 1158–1165 (1975).
13. A. L. Burka, Allowance for the temperature dependence of the absorption coefficient in analysis of coupled radiative-plus-conductive heat transfer, *Heat Transfer—Sov. Res.* **11**(5), 14–21 (1979).
14. C. K. Hsieh and K. C. Su, Thermal radiative properties of glass from 0.32 to 206 μm, *Solar Energy* **22**, 37–43 (1979).
15. Tan He Ping, M. Ferre and M. Lallemand, Transfert radiatif dans NO_3K fondu et la fonte vitreuse de B_2O_3, *Rev. Phys. Applic.* **22**, 125–138 (1987).
16. H. C. Hottel and A. F. Sarofim, *Radiative Transfer*. McGraw-Hill, New York (1967).
17. T. Kunc, M. Lallemand and J. B. Saulnier, Some new developments on coupled radiative–conductive heat transfer in glasses—experiments and modelling, *Int. J. Heat Mass Transfer* **27**, 2307–2319 (1984).
18. Tan He Ping and M. Lallemand, Transient combined conductive–radiative heat transfer in semi-transparent materials with flux and mixed boundary conditions for semi-transparent or opaque frontiers. Eurotherm Seminar No. 1, Mons, Belgium, 7–8 March (1988).
19. S. V. Patankar, *Numerical Heat Transfer and Fluid Flow*. McGraw-Hill, New York (1980).
20. Tan He Ping and M. Lallemand, Transfert couplé rayonnement–conduction instationnaire dans les verres. IIIième JIHT, Lyon-Villeurbanne, France, pp. 350–357 (1987).
21. E. E. Anderson and R. Viskanta, Spectral and boundary effects on coupled conduction–radiation heat transfer through semi-transparent solids, *Wärme- und Stoffübertr.* **1**, 14–24 (1973).

APPENDIX. EXPRESSIONS OF THE SOURCE TERMS

A.1. *Opaque frontiers*

$$\Phi_i^r = \sigma \sum_{k=1}^{NBA} n_{k,M}^2 \Bigg\{ \varepsilon_{2,k}(S_2V_i)_{k,o-o}^s(a_{k,T_{s2}}T_{s2}^4 - a_{k,T_i}T_i^4) + \varepsilon_{1,k}(S_1V_i)_{k,o-o}^s(a_{k,T_{s1}}T_{s1}^4 - a_{k,T_i}T_i^4) + \sum_{j=2}^{NM-1}(V_jV_i)_{k,o-o}^s(a_{k,T_j}T_j^4 - a_{k,T_i}T_i^4)\Bigg\} \quad (2 \leqslant i \leqslant NM-1). \tag{A1}$$

A.2. *Semi-transparent and opaque frontiers*

$$\Phi_i^r = \sigma \sum_{k=1}^{NBA} n_{k,M}^2 \Bigg\{ \varepsilon_{2,k}(S_2V_i)_{k,t-o}^s(a_{k,T_{s2}}T_{s2}^4 - a_{k,T_i}T_i^4) + (V_iS_{-\infty})_{k,t-o}^s(a_{k,T_{s-\infty}}T_{s-\infty}^4 - a_{k,T_i}T_i^4) + \sum_{j=2}^{NM-1}(V_jV_i)_{k,t-o}^s(a_{k,T_j}T_j^4 - a_{k,T_i}T_i^4)\Bigg\} \quad (2 \leqslant i \leqslant NM-1). \tag{A2}$$

TRANSFERT DE CHALEUR RAYONNEMENT–CONDUCTION INSTATIONNAIRE DANS LES VERRES PLATS SOUMIS A DES CONDITIONS AUX LIMITES DE TEMPERATURE, DE FLUX ET MIXTES

Résumé—Le problème monodimensionnel du transfert de chaleur instationnaire couplé rayonnement–conduction dans les milieux semi-transparents non gris (plus spécialement les verres) a été traité par l'analyse nodale et la méthode des zones de Hottel étendue aux concepts de l'optique géométrique pour des conditions aux limites thermiques et radiatives variées. Le problème du couplage a été étudié pour le cas des températures imposées, des lois d'échange radiatif et convectif imposées ainsi que pour le cas mixte et ce, dans le cas d'interfaces opaques, ou à réflexions vitreuses et spéculaires. Les effets des paramètres d'influence, nombre de Planck, nombre de Biot, nombre de Fourier, émissivités de la couche et indice de réfraction du milieu ont été examinés. Deux applications de la modélisation numérique ont été considérées : la prévision du comportement temporel d'un parebrise d'avion spatial durant la phase de rentrée et la simulation du transfert instationnaire dans une fonte de verre soumis d'un côté au contact d'un bain métallique et de l'autre échangeant de la chaleur par convection et rayonnement.

TRANSIENTER WÄRMEAUSTAUSCH DURCH STRAHLUNG UND LEITUNG IN GLASSCHEIBEN BEI UNTERSCHIEDLICHEN RANDBEDINGUNGEN

Zusammenfassung—Es wird ein Knotenmodell entwickelt, das auf Hottel's Zonenverfahren basiert und mit der Strahlungsverlauf-Methode erweitert ist. Damit wird der kombinierte eindimensionale, transiente Wärmeaustausch durch Strahlung und Leitung in nicht-grauen, semitransparenten Materialien, hauptsächlich jedoch Glas, bei unterschiedlichen thermischen Randbedingungen untersucht. Probleme bei der Verknüpfung der aufgeprägten Temperaturen mit den Wärmeübergangsbeziehungen für Strahlung und Konvektion sowie den gemischten thermischen Randbedingungen werden sowohl für opake als auch für spiegelnde, glasartige Oberflächen gelöst. Der Einfluß der maßgeblichen Parameter wie Planck-Zahl, Biot-Zahl, Fourier-Zahl, Emissionsverhältnis der Scheibe sowie der Brechzahl des Stoffes werden betrachtet. Zwei unterschiedliche Anwendungen werden numerisch untersucht: Zum einen wird das zeitabhängige Aufheizverhalten des thermischen Schutzschildes an einem Raumfahrzeug beim Eintauchen in die Erdatmosphäre berechnet und zum anderen der transiente Wärmeaustausch einer Glasschmelze, die an ihrer Unterseite mit einer Metallschmelze in Kontakt ist und an deren Oberseite Wärmeverluste durch Strahlung und Konvektion auftreten.

НЕСТАЦИОНАРНЫЙ ЛУЧИСТО-КОНВЕКТИВНЫЙ ТЕПЛОПЕРЕНОС В ПЛОСКИХ СТЕКЛАХ ПРИ ЗАДАННЫХ ТЕМПЕРАТУРЕ, ПЛОТНОСТИ ТЕПЛОВОГО ПОТОКА И СМЕШАННЫХ ГРАНИЧНЫХ УСЛОВИЯХ

Аннотация—Для решения одномерной задачи нестационарного смешанного лучисто-конвективного теплопереноса в несерых полупрозачных материалах (стеклах) при различных тепловых и радиационных граничных условиях проводится анализ, основанный на зональном методе Хоттеля с использованием метода лучевой индикации. Для непрозрачных, а также для стекловидных межфазных границ с зеркальным отражением рассмотрены задачи взаимодействия при заданных температурах, законах лучисто-конвективного теплообмена и смешанных тепловых условиях. Исследованы изменения параметров изучения, чисел Планка, Био и фурье, излучательной способности пластины, а также коэффициента преломления среды. Рассмотрены два случая численного моделирования: для расчета поведения кварцевого ветрового стекла, установленного на космическом корабле при входе в плотные слои атмосферы, и для определения нестационарого теплопереноса в расплаве стекла, с одной сторны контактирующего с металлической ванной, а с другой стороны находящегося в условиях радиациоино-конвективного теплообмена.